Propulsion Systems for e-VTOL Aircraft

Technical Milestone Report

Samuel Drury

Supervised by: Dr Sam Grimshaw; Dr James Taylor

Introduction

Electric Vertical Take-Off and Landing (e-VTOL) vehicles are playing an increasingly important role in accelerating the path to zero-carbon flight, alongside bringing shorter commuting times at an affordable price [1]. There is a choice to be made when selecting propulsors: while the simplicity of propellers make them an attractive option, hovering performance and efficiency can be increased by using ducted fans [2]. Additionally, ducting the fans reduces the noise and brings an added safety benefit by shielding the rotating components.

This report details the design methods used to generate ducted fans and the experiments performed to quantify the increased performance over two different propellers. Following successful static tests, a set of four ducted fans are printed in Polylactic Acid (PLA) using an Ultimaker (3D printer) to develop a flying test bed (Fig. 1), whereby dynamic measurements can be taken to initially assess hover and stability performance.

Following disruptions due to the COVID-19 pandemic, the future work section explores how the project plan has changed and now focuses on improving the design process by developing and including a loss model. This will account for sources of inefficiency and assess design trade-offs, allowing the open design space to be explored further yet quickly.

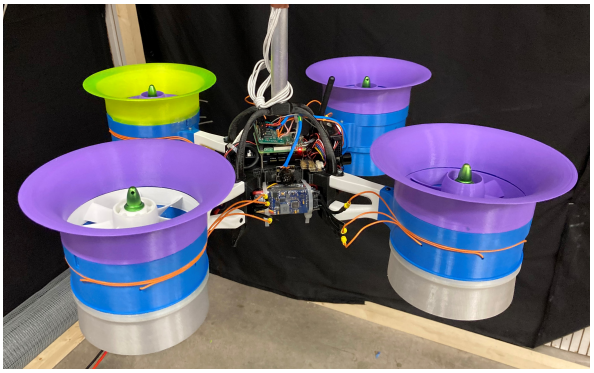

Figure 1: Flying test bed

Design Method

2.1 Fan Design

The following methodology to design ducted fans builds on work completed by previous students [3]. It starts by considering a control volume to develop mean line velocity triangles, then develops a spanwise velocity distribution using radial equilibrium, and finally develops spanwise chord and diffusion factor distributions that, with constant deviation, fix the blade geometry.

2.1.1 Assumptions

To simplify the physics governing the fluid dynamics in the flow path, several assumptions are invoked that aid blade design. The flow is assumed to be incompressible and isentropic, and modelled to have no inlet or exit swirl. Additionally, the mean-line for the flow passage is defined at a radius with equal mass flow above and below (Eqn. 2.3). At the exit, the static pressure is assumed to be atmospheric and the exit flow area equal to the duct area.

2.1.2 Generating Blade Geometry

T_T	10 N
r_h	20 mm
r_c	60 mm
σ	1.13
ϕ	0.8
ψ	0.25
Ω	7900 RPM
M_f	1.50
N_r	8
N_s	7

Table 1: 1D Design Parameters

Appropriate values of flow coefficient ϕ and exit duct area ratio σ are selected from previous work [3, 4], and used alongside the geometry constraints (hub and casing radii r_h, r_c) given in Table 1. The thrust requirement T_T is set such that the RPM is suitable for small hobby motors.

Using the Steady Flow Momentum and Energy equations, the axial velocity V_x and blade rotational speed Ω are determined. Next, the spanwise velocity distribution (Fig. 2a) based on a mixed vortex design is determined from radial equilibrium, and using the stage loading coefficient for isentropic flow (Eqn. 2.4) yields the flow angles (Figs. 2b and 2c). Lieblein's correlation [5] for diffusion factor and a specified aspect ratio set the mean-line chord and pitch, which are used in Carter's empirical relation [6] to determine the mean line deviation. The mean line pitch is used to determine the required number of blades (N_r, N_s) for the rotor and stator rows.

A chord distribution (Fig. 2d) that yields a constant deviation across the span is determined using Carter's rule again, and similarly Lieblein's correlation relates the chord distribution to the diffusion factor distribution (Fig. 2e), found to be below a predetermined threshold of 0.45, reducing the risk of stall. From the blade metal angles, blade profiles are calculated using sections from Maffioli [7].

Finally, to minimise end-wall losses and extend the propulsor operating range through limiting separation, suitable values of sweep and lean are selected from work by Taylor & Miller [8].

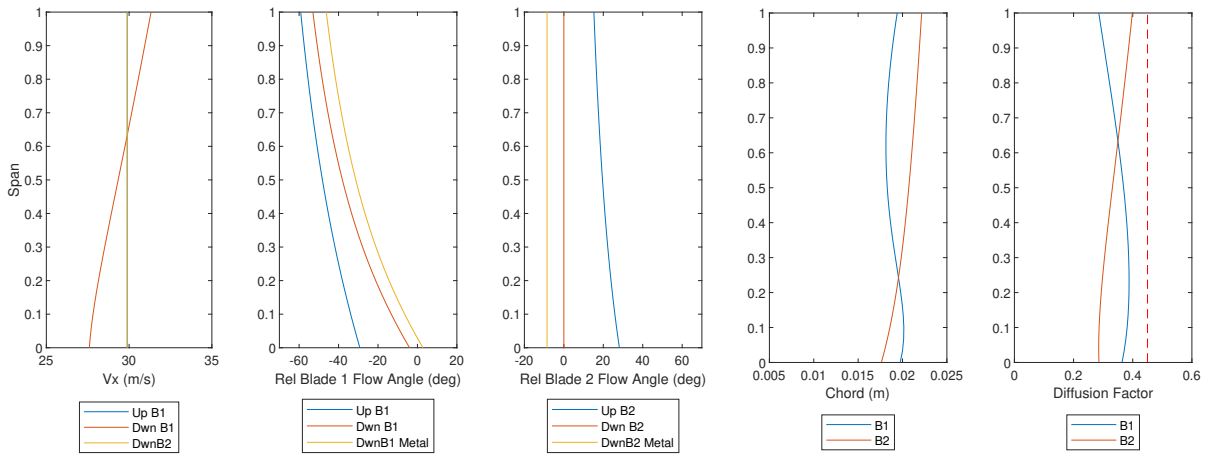

(a) (b) (c) (d) (e)

Figure 2: Design charts showing spanwise distributions for: axial velocity (a), flow and metal angles (b,c), chord (d), and diffusion factor (e)

2.2 Determining Performance

2.2.1 Data Collection

Detailed descriptions for the methods of data collection are listed in the work done by a previous student [3]. In summary, an on-board Raspberry Pi 3+ (RPi3+) module running Python scripts allows RPM to be measured through an infra-red (IR) sensor and the thrust through a load cell (static test stand only), and this data is exported over WiFi using Secure Shell (SSH) protocol. A pressure transducer connected through Ethernet enables pressure readings to be taken from tappings along the ducted fan casing. Finally, the flight control hardware (Pixhawk 4) has accompanying software (QGroundControl) to control the fan(s), where a continuous feed including voltage and current measurements can be processed to obtain the input power.

2.2.2 Figure of Merit

When hovering, the conventional propulsive efficiency would equate to zero, therefore Pereira defines a Figure of Merit (FOM) as in Eqn. 2.1, which reduces to Eqn. 2.2 upon substitution for a ducted fan operating isentropically [2]. For a propeller, the ideal FOM is equal to 1.

$$M_f = \frac{T_T}{P}\sqrt{\frac{T_T}{2\rho A_x}} \tag{2.1}$$

$$M_f = \sqrt{2\sigma} \tag{2.2}$$

2.2.3 Static tests with single ducted fan

Mounting the ducted fan or propeller to a fixed reference through a load cell allows the four measurements (Power, RPM, thrust, pressures (ducted fan only)) to be taken, enabling the relative performance of propulsors to be quantified.

Fig. 3 shows pressure tapping locations, and equations 2.5 and 2.6 relate the pressures to values of ϕ and ψ calculated at the mean line.

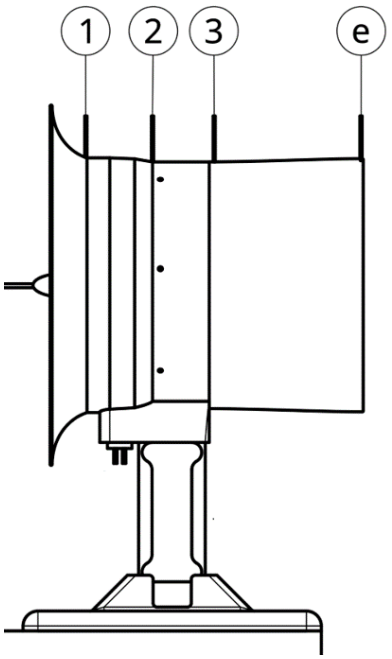

Figure 3: Static test stand with pressure tapping locations

$$r_m = \sqrt{\frac{r_h^2 + r_c^2}{2}} \tag{2.3}$$

$$\psi = \frac{\phi^2}{2\sigma^2} \tag{2.4}$$

$$\phi_m = \frac{V_{x,m}}{U_m} = \frac{V_{x,c}}{\Omega r_m} \approx \sqrt{\frac{(p_0 - p_1)_c}{\frac{1}{2}\rho(\Omega r_m)^2}} \tag{2.5}$$

$$\psi_m = \frac{p_{03} - p_0}{\rho(U_m)^2} = \frac{p_3 + \frac{1}{2}\rho(V_{x,m})^2 - p_0}{\rho(U_m)^2}$$

$$\psi_m \approx \frac{(p_3 - p_0)_c}{\rho(\Omega r_m)^2} + \frac{1}{2}\phi_m^2 \tag{2.6}$$

The modular nature of the ducted fans means the exit area ratio (σ) can be varied by changing the outer duct and inner tail cone to alter the operating point of the fan. Reducing area ratio limits the mass flow, reducing the flow coefficient ϕ and theoretically increasing the stage loading coefficient ψ, providing the fan does not stall. Increasing area ratio increases the flow coefficient, and a further increase in flow coefficient is achieved by placing a box fan upstream, along with a pitot tube to measure the new stagnation pressure, previously assumed to be atmospheric.

2.2.4 Dynamic tests with flying test bed

With four ducted fans mounted onto the chassis (Fig. 1), in-flight measurements can be taken remotely using the RPM IR sensor, casing pressure tappings, and the on-board Pixhawk 4 hardware with inbuilt accelerometers, gyros and ultrasound position sensors. Along with equating the ducted fan thrust to a quarter of the test bed weight, hover performance can be quantified, and the Pixhawk 4 sensor data can support conclusions of stability performance, for example measuring the motor response time in correcting position.

Up to three additional ADC breakout boards can be added to the RPi3+ to give a possible 30 ports for pressure sensors [9]. These can be used to analyse the flow in detail around the inlet/exit ducts and around the annulus, to quantify any separation.

Experimental Results

3.1 Ducted Fan Figure of Merit

Using measurements of thrust, RPM and input power (measured as Pixhawk 4 power consumption) from the static test stand, FOMs for three propulsors are shown in Table 2. As expected, the Advanced Precision Composites (APC) VTOL-optimised propeller outperforms the cheaper stock propeller from Amazon by 5%. The ducted fan has a FOM 63% greater than the APC propeller, yet has a higher ideal FOM (Eqn. 2.2). Nonetheless, the efficiency is higher, proving an improved aerodynamic efficiency for the ducted fan, considering the system efficiency will be comparable with the propeller tests due to using the same motors.

Propulsor	Measured FOM	Ideal FOM	Efficiency
Amazon propeller	0.41	1	41%
APC propeller	0.43	1	43%
Ducted fan	0.70	1.50	47%

Table 2: Comparing FOMs for three different propulsors

3.2 Ducted Fan Characteristic

Figure 4 shows the mean line characteristic of the ducted fan, with non-dimensional pressure rise (stage loading, ψ) plotted against non-dimensional mass flow rate (flow coefficient, ϕ).

Equation 2.4 relates the flow and loading coefficients to the exit area ratio for isentropic flow, and since the flow coefficient is set to be uniform at $\phi = 0.8$ across the span at inlet,

this yields the theoretical design point. Flow irreversibilities arising from friction on the blades and hub/casing end walls result in lower momentum wakes forming from trailing edges and around the shroud gaps. As such, the actual design point has a lower stage loading coefficient.

Neglecting points where the compressor stalls, the stage loading increases as the flow coefficient reduces, as expected with typical compressor characteristics [10]. A key observation is that the design point has a comfortable stall margin, increasing stability for off-design conditions. A stalled compressor can be identified by an increase in noise and occurs when the throttle (exit area ratio) is reduced to a point where the stagnation pressure rise falls off due to flow separation.

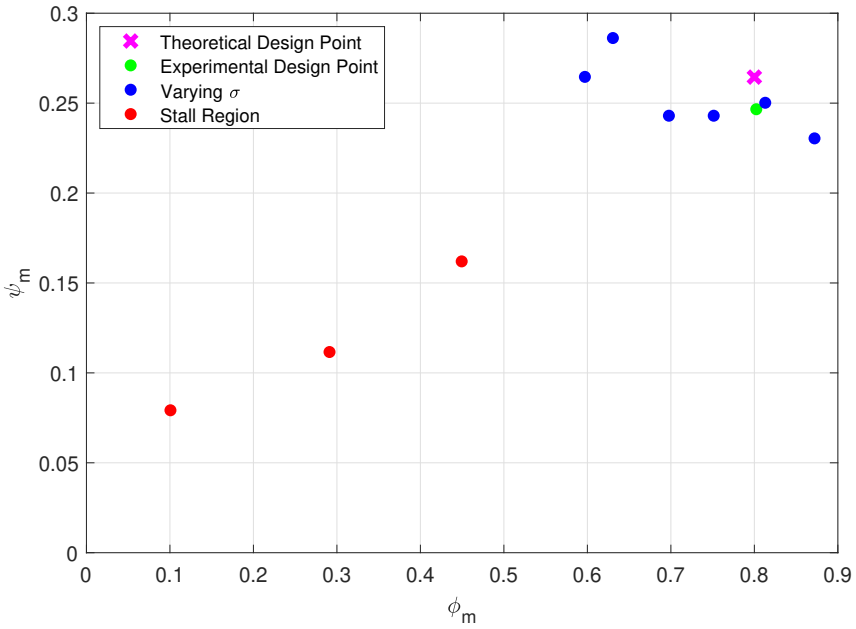

Figure 4: Ducted fan characteristic: loading coefficient vs flow coefficient

Conclusions

1. 3D printing is a suitable manufacturing method to produce propulsor designs generated through 1D and 2D fluid flow theory with added 3D features.

2. Ducted fans outperform propellers, with a 63% increase in Figure of Merit relative to a VTOL-optimised propeller.

3. Throttling a ducted fan by varying the exit area ratio is a successful method to obtain a fan characteristic. This helps validate the design theory and show there is a margin in the operating point before the fan stalls.

4. Using a previously developed modular flying test bed but now with ducted fans instead of propellers, successful test flights prove that measurements of performance and stability can be taken.

5. Losses contribute to an overall ducted fan efficiency of 47%, so incorporating a loss model into the design will help to optimise for aerodynamic efficiency.

Future Work

Due to the ongoing COVID-19 pandemic, restrictions on lab access render plans to continue developing the flying test bed infeasible at present. Existing assumptions in the design help narrow the vast design space, yet trade-offs between properties such as: aerodynamic and propulsive efficiency, figure of merit, and tip Mach number can't be evaluated due to assuming isentropic, incompressible flow. A better design tool is required to better explore the design space, which will be achieved through developing a loss model that accounts for: profile losses on the surface of blades; tip losses for leakage flow between the rotor shroud and casing wall; and hub and casing end wall losses. Using this model in the design process allows a multi-parameter optimisation to take place, taking potential inputs of: casing and hub diameters, exit area ratio, flow coefficient, vortex exponent and diffusion factor. The generated matrix of improved designs will be compared to aerodynamic efficiencies produced through CFD software Turbostream.

References

[1] R. Whittle. "Air Mobility Bonanza Beckons Electric VTOL Developers". *Vertiflite* March/April (2017).

[2] J. L. Pereira. "Hover and wind-tunnel testing of shrouded rotors for improved micro air vehicle design". Tech. rep. (2008).

[3] J. Eriksen. "Propulsion Systems for VTOL Electric Vehicles". Cambridge University Engineering Department (2020).

[4] M. McEveley. "Propulsion Systems for VTOL Electric Vehicles". Cambridge University Engineering Department (2020).

[5] S. Lieblein, F. C. Schwenk, and R. L. Broderick. "Diffusion factor for estimating losses and limiting blade loadings in axial flow compressor blade elements." *NACA R.M.* E53 D01 (1953).

[6] A. Carter. *The Low Speed Performance of Related Aerofoils in Cascade*. Current papers. Ministry of Supply, National Gas Turbine Establishment, 1950.

[7] A. Maffioli, C. Hall, and S. Melvin. "Aerodynamics of low reynolds number axial compressor sections". *53rd AIAA Aerospace Sciences Meeting* (2015).

[8] J. Taylor and R. Miller. "Competing three-dimensional mechanisms in compressor flows" (2016).

[9] ABelectronicsUK. *ADC Differential Pi*. URL: `https://www.abelectronics.co.uk/p/65/adc-differential-pi-raspberry-pi-analogue-to-digital-converter` (visited on 12/01/2021).

[10] S. L. Dixon and C. A. Hall. *Fluid Mechanics and Thermodynamics of Turbomachinery*. Seventh edition. Butterworth-Heinemann, 2014.